



HAL
open science

Recognition of the *Magnaporthe oryzae* effector AVR-Pia by the decoy domain of the rice NLR immune receptor RGA5

Diana Ortiz, Karine de Guillen, Stella Cesari, Veronique Chalvon-Poulier, Jérôme Gracy, André Padilla, Thomas Kroj

► To cite this version:

Diana Ortiz, Karine de Guillen, Stella Cesari, Veronique Chalvon-Poulier, Jérôme Gracy, et al.. Recognition of the *Magnaporthe oryzae* effector AVR-Pia by the decoy domain of the rice NLR immune receptor RGA5. *The Plant cell*, 2017, 29 (1), pp.156-168. 10.1105/tpc.16.00435 . hal-01608403

HAL Id: hal-01608403

<https://hal.science/hal-01608403>

Submitted on 26 May 2020

HAL is a multi-disciplinary open access archive for the deposit and dissemination of scientific research documents, whether they are published or not. The documents may come from teaching and research institutions in France or abroad, or from public or private research centers.

L'archive ouverte pluridisciplinaire **HAL**, est destinée au dépôt et à la diffusion de documents scientifiques de niveau recherche, publiés ou non, émanant des établissements d'enseignement et de recherche français ou étrangers, des laboratoires publics ou privés.

Copyright



Recognition of the *Magnaporthe oryzae* Effector AVR-Pia by the Decoy Domain of the Rice NLR Immune Receptor RGA5^{OPEN}

Diana Ortiz,^{a,1} Karine de Guillen,^{b,1} Stella Cesari,^{a,c} Véronique Chalvon,^a Jérôme Gracy,^b André Padilla,^b and Thomas Kroj^{a,2}

^aINRA, BGPI, Biology and Genetics of Plant-Pathogen Interactions, Campus International de Baillarguet, 34398 Montpellier, France

^bCNRS UMR 5048, INSERM U1054, Centre de Biochimie Structurale, Université Montpellier, 34090 Montpellier, France

^cCSIRO Agriculture Flagship, Canberra ACT 2601, Australia

ORCID IDs: 0000-0002-9778-0327 (J.G.); 0000-0001-9702-4612 (A.P.); 0000-0002-3752-1788 (T.K.)

Nucleotide binding domain and leucine-rich repeat proteins (NLRs) are important receptors in plant immunity that allow recognition of pathogen effectors. The rice (*Oryza sativa*) NLR RGA5 recognizes the *Magnaporthe oryzae* effector AVR-Pia through direct interaction. Here, we gained detailed insights into the molecular and structural bases of AVR-Pia-RGA5 interaction and the role of the RATX1 decoy domain of RGA5. NMR titration combined with *in vitro* and *in vivo* protein-protein interaction analyses identified the AVR-Pia interaction surface that binds to the RATX1 domain. Structure-informed AVR-Pia mutants showed that, although AVR-Pia associates with additional sites in RGA5, binding to the RATX1 domain is necessary for pathogen recognition but can be of moderate affinity. Therefore, RGA5-mediated resistance is highly resilient to mutations in the effector. We propose a model that explains such robust effector recognition as a consequence, and an advantage, of the combination of integrated decoy domains with additional independent effector-NLR interactions.

INTRODUCTION

Plant disease resistance largely relies on inducible immune responses that are triggered upon receptor-mediated recognition of pathogen molecules and that often involve a localized programmed cell death called the hypersensitive response (HR). Particularly important are NLRs, cytoplasmic nucleotide binding oligomerization domain-like receptors with a multidomain architecture composed of a C-terminal leucine-rich repeat domain and a central nucleotide binding domain (Takken and Goverse, 2012; Jacob et al., 2013; Qi and Innes, 2013). Most NLRs carry in addition an N-terminal coiled-coil or Toll/interleukin-1 receptor domain that have both been reported to mediate NLR homo-complex formation and to be crucial for the activation of downstream signaling (Bernoux et al., 2011; Maekawa et al., 2011). Plant NLR proteins specifically recognize pathogen-derived effectors that act inside plant cells (Cui et al., 2015).

Traditionally, both effector recognition and activation of resistance signaling are thought to be mediated by single plant NLRs, but recent studies revealed an increasing number of cases where different NLRs cooperate in pathogen recognition and resistance (Eitas and Dangl, 2010; Cesari et al., 2014a). Frequently, the genes coding for these paired NLRs occur in a paired, inverted tandem arrangement in the genome. In the rare cases

investigated in more detail, the NLR pairs seem to act as hetero-complexes where only one of the paired NLRs acts directly in effector recognition while the other is crucial for the activation of downstream signaling (Williams et al., 2014; Cesari et al., 2014b). In other cases, helper NLRs that act downstream of several NLRs with different recognition specificities were shown to be required for resistance and pathogen detection (Gabriëls et al., 2007; Bonardi et al., 2011; Wu et al., 2016).

Some plant NLRs recognize effectors in an indirect manner. They detect either a modification of the effector's host target protein called a "guardee" or modifications of a host protein that mimics the effector target and is called a "decoy" (van der Hoorn and Kamoun, 2008). Effectors can also be recognized in a direct manner by binding, either alone, or in complex with a cofactor that may be a guardee or a decoy, to the NLRs (Takken and Goverse, 2012; Collier and Moffett, 2009). In these cases, the leucine-rich repeat domain plays a crucial role in recognition specificity and has frequently been shown to mediate direct effector binding (Ellis et al., 2007; Krasileva et al., 2010; Jia et al., 2000). Alternatively, direct effector recognition can be mediated by non-canonical domains integrated into NLRs at low frequencies (Kanzaki et al., 2012; Sarris et al., 2015; Maqbool et al., 2015; Le Roux et al., 2015; Cesari et al., 2013). Recent work led to the hypothesis that these highly diverse integrated domains are mimics of effector targets and can therefore be considered as integrated decoy domains (Le Roux et al., 2015; Sarris et al., 2015; Cesari et al., 2014a). However, the molecular mechanisms of effector recognition by integrated domains and the advantages of this mode of recognition remain largely unknown.

Rice blast, caused by the fungus *Magnaporthe oryzae*, is a highly destructive crop disease and a serious threat for food security (Pennisi, 2010; Dean et al., 2012; Skamnioti and Gurr,

¹ These authors contributed equally to this work.

² Address correspondence to thomas.kroj@inra.fr.

The author responsible for distribution of materials integral to the findings presented in this article in accordance with the policy described in the Instructions for Authors (www.plantcell.org) is: Thomas Kroj (thomas.kroj@inra.fr).

^{OPEN}Articles can be viewed without a subscription.

www.plantcell.org/cgi/doi/10.1105/tpc.16.00435

2009). NLR-mediated pathogen recognition is the major mechanism in rice blast resistance. Among 25 different blast resistance genes cloned over the last 20 years, 24 code for NLRs (Liu et al., 2014). Blast resistance is frequently conferred by paired NLRs with clustered tandem organization in the genome. Among these, the NLR pair RGA4/RGA5 encoded by the *Pi-CO39/Pia* resistance locus has been developed as a model for molecular understanding of paired NLRs (Okuyama et al., 2011; Césari et al., 2013, 2014b). In this pair, RGA4 acts as a constitutively active disease resistance and cell death inducer that is repressed by RGA5 in the absence of pathogen (Césari et al., 2014b). In addition to its repressor function, RGA5 acts as a receptor for the *M. oryzae* effectors AVR1-CO39 and AVR-Pia. Direct binding of RGA5 to these effectors results in derepression of RGA4 and activation of resistance signaling. Effector binding involves the unconventional C-terminal related to ATX1 (RATX1) domain of RGA5, which is similar to a heavy metal-associated (HMA) domain protein from *Saccharomyces cerevisiae* that acts as a cytoplasmic copper chaperone (Césari et al., 2013). The RATX1 domain of RGA5 is dispensable for RGA4 repression and seems exclusively dedicated to effector binding (Césari et al., 2014b). Since the rice RATX1/HMA protein Pi21 is a blast susceptibility factor required for full disease development (Fukuoka et al., 2009), it has been hypothesized that AVR1-CO39 and AVR-Pia target RATX1/HMA proteins for disease development and that the RATX1 domain is an integrated decoy domain (Césari et al., 2014b, 2013).

An HMA domain 53% identical to the RGA5 RATX1 domain is also present in another rice (*Oryza sativa*) NLR, Pik-1, which acts together with the NLR Pik-2 in the specific recognition of the *M. oryzae* effector AVR-Pik. Like in RGA5, this domain acts by directly binding the effector and is crucial for its recognition (Kanzaki et al., 2012). However, contrary to the C-terminal RATX1 domain of RGA5, the HMA domain of Pik-1 is located between the coiled-coil and nucleotide binding domains, indicating independent integration of the same domains in the two unrelated NLRs (Césari et al., 2013). Recently, the determination of the crystal structure of the AVR-PikD/Pikp-1 HMA domain complex allowed the precise identification of the AVR-PikD surface mediating binding to the Pikp-1 HMA domain (Maqbool et al., 2015).

Although AVR-Pik, AVR-Pia, and AVR1-CO39 do not share sequence similarities, they share a highly similar three-dimensional structure characterized by a six β -sandwich fold also present in two other effectors: AvrPiz-t from *M. oryzae* and ToxB from the wheat pathogenic fungus *Pyrenophora tritici repentis* (Zhang et al., 2013; de Guillen et al., 2015; Maqbool et al., 2015; Nyarko et al., 2014). The corresponding, structurally related *Magnaporthe* Avr and ToxB effectors were termed MAX effectors. MAX effectors are present in other sometimes only distantly related phytopathogenic fungi and the MAX effector family underwent strong expansion in *M. oryzae* where it accounts for roughly 10% of the effectors (de Guillen et al., 2015).

In this study, we investigated the molecular and structural bases of AVR-Pia recognition by RGA5 with a focus on the role of the RATX1 domain in effector binding and recognition. We show that AVR-Pia interacts with the RGA5_{RATX1} domain through a precise surface that shares some similarity, but also important differences, with the HMA binding surface of AVR-Pik. We demonstrate that binding to the RATX1 domain is required for effector recognition

but that strong reduction in binding strength is tolerated. We also provide evidence that the RATX1 domain is not required for association of AVR-Pia with RGA5 and that it associates with additional sites in the NLR, which could explain the high tolerance of recognition to reduced AVR-Pia-RATX1 binding strength. Based on our results, we propose a model illustrating the advantages of effector recognition by integrated decoy domains as well as additional simultaneously occurring interactions with NLR receptors.

RESULTS

The F24S and T46N Substitutions in the Nonrecognized AVR-Pia-H3 Allele Affect Surface Properties but Not Structure

We previously described the naturally occurring AVR-Pia allele AVR-Pia-H3 that carries two nonsynonymous polymorphisms leading to the F24S and T46N substitutions (Césari et al., 2013). *M. oryzae* isolates carrying the AVR-Pia-H3 allele are virulent on rice varieties carrying the *Pia* resistance locus and AVR-Pia-H3 does not interact in yeast two-hybrid (Y2H) assays with the C-terminal part of the rice NLR immune receptor RGA5 containing the RATX1 domain (RGA5_{C-ter}). The NMR structure of AVR-Pia showed that both the F24 and T46 residues are surface exposed and suggested that the corresponding substitutions affect only AVR-Pia surface properties without major structural rearrangements (de Guillen et al., 2015).

To test this hypothesis, the structures of AVR-Pia-H3 and the single mutants AVR-Pia^{F24S} or AVR-Pia^{T46N} were analyzed by NMR spectroscopy. We performed sequential assignments using ¹⁵N-labeled AVR-Pia samples, and the ¹³C α and ¹³C β assignments were performed using ¹³C-¹H 2D experiments with a ¹³C-natural abundance sample in D₂O (Supplemental Methods). When compared with AVR-Pia wild type, ¹H-¹⁵N chemical shifts differed more in AVR-Pia-H3 than in AVR-Pia^{F24S} or AVR-Pia^{T46N} single mutants (Figure 1A). The NMR structure of AVR-Pia-H3 proved to be very similar to the structure of AVR-Pia (PDB code 5JHJ) (Figure 1B; Supplemental Table 1 and Supplemental Figure 1). The backbone RMSD for superposition of the AVR-Pia and AVR-Pia-H3 structures is 1.53 Å and drops to 0.93 Å when the β 1- β 2 loop is excluded and the superposition starts at residue R23. Like the AVR-Pia wild-type protein, AVR-Pia-H3 shows the MAX-effector topology characterized by six antiparallel β -strands (Figure 1C). The ¹H-¹⁵N chemical shift data for AVR-Pia^{F24S} and AVR-Pia^{T46N} indicate that both single mutants probably also keep the MAX-effector fold (Figure 1A). We also compared ¹⁵N relaxation data between AVR-Pia and AVR-Pia-H3, by a Model-Free analysis. The order parameter (S^2) ranges from 0 for a flexible residue to 1 for a rigid one and reflects the amplitude of the fast internal motion of the H^N-N bond vectors in the picoseconds-to-nanosecond time range. Our analysis indicated that both AVR-Pia^{wt} and AVR-Pia-H3 have rigid structures with average S^2 values of 0.8 and similar S^2 profiles, indicating similar protein dynamics (Supplemental Figure 2).

The 3D structure of AVR-Pia-H3 therefore supports the conclusion that the F24S and T46N substitutions do not result in

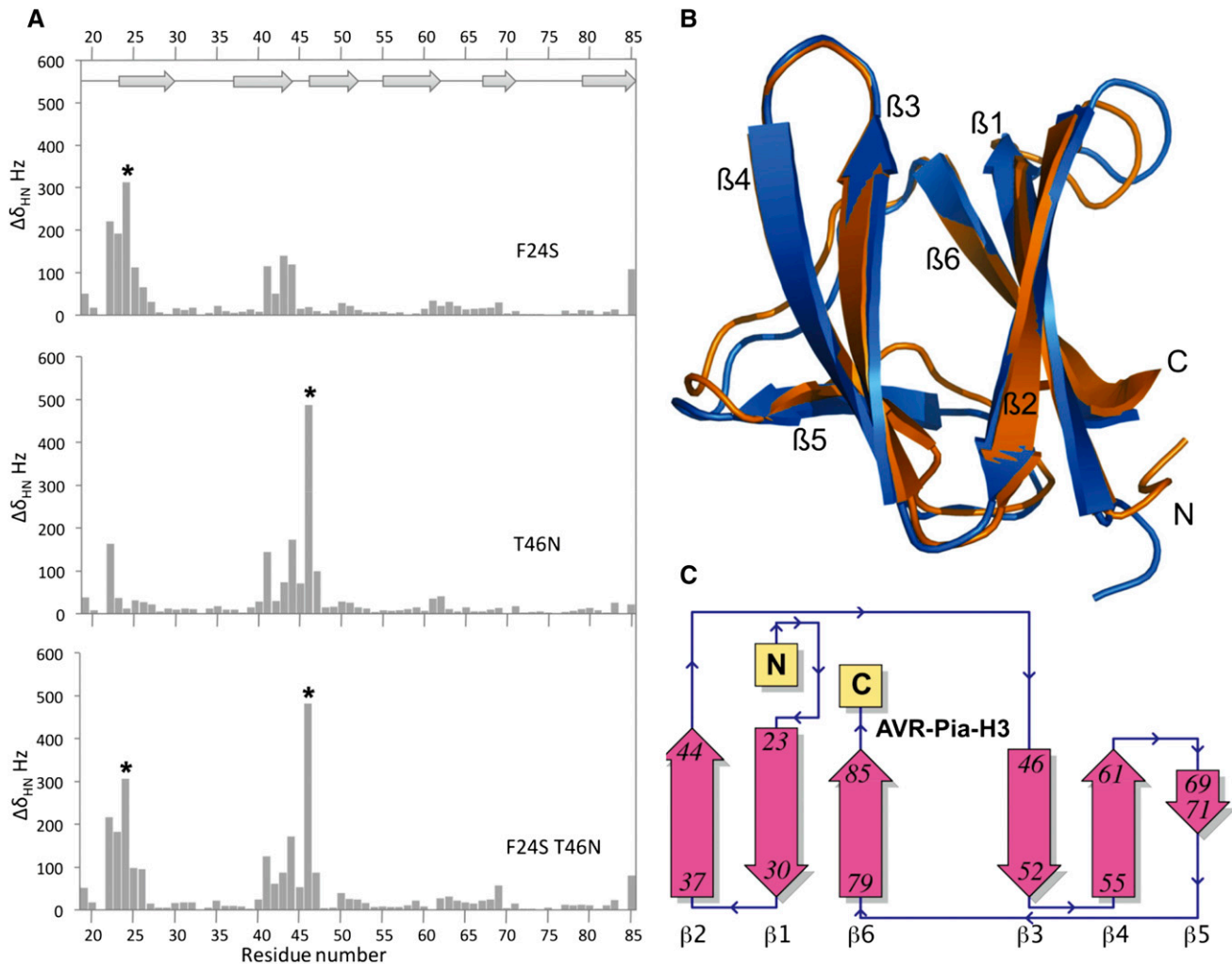


Figure 1. The AVR-Pia-H3 NMR Structure Is Similar to the Structure of Wild-Type AVR-Pia.

(A) Chemical shift differences ($\Delta\delta_{\text{HN}}$) from the comparison of ^{15}N -HSQC of AVR-Pia wild type and mutants F24S, T46N, or F24S T46N (AVR-Pia-H3). The β -strand assignments from the AVR-Pia^{wt} structure are indicated on the top and polymorphic residues by an asterisk.

(B) Structure overlay of AVR-Pia (blue) and AVR-Pia-H3 (orange).

(C) Topology of the AVR-Pia-H3 structure.

conformational changes but rather alter AVR-Pia surface properties required for strong interaction with the RATX1 domain of RGA5 (RGA5_{RATX1}) and disease resistance activation.

AVR-Pia Binds RGA5_{RATX1} with Intermediate Affinity

To characterize the AVR-Pia/RGA5_{RATX1} interaction, *in vitro* binding assays with recombinant RGA5_{RATX1} and AVR-Pia or AVR-Pia-H3 were performed using isothermal calorimetry (ITC). For AVR-Pia, specific and direct binding to RGA5_{RATX1} with a one-site model and a K_d of 7.8 μM was detected (Figure 2A). For AVR-Pia-H3, no binding was detected under identical conditions, indicating that its affinity to RGA5_{RATX1} was drastically reduced. To determine the contribution of the individual substitutions, F24S and T46N, to the reduction in binding, AVR-Pia^{F24S} and AVR-Pia^{T46N} single mutants were

characterized for RGA5_{RATX1} binding. AVR-Pia^{F24S} showed no binding, while AVR-Pia^{T46N} seemed to bind very weakly. However, the affinity was so weak that no K_d value could be determined.

β -Strands 2 and 3 and Residues R23, F24, E56, and E58 Constitute a Candidate RGA5_{RATX1}-Interaction Surface in AVR-Pia

To test the hypothesis that the residues F24 and T46 are part of the AVR-Pia surface mediating direct contacts to RGA5_{RATX1} and to identify other residues in direct contact with RGA5_{RATX1} or located in the close vicinity of the binding interface, NMR titration experiments were performed. This technique consists of recording the ^1H - ^{15}N -HSQC NMR spectra of ^{15}N -labeled AVR-Pia in the presence of increasing amounts of unlabeled RGA5_{RATX1}. When protein-protein binding occurs, it modifies the chemical environment of the

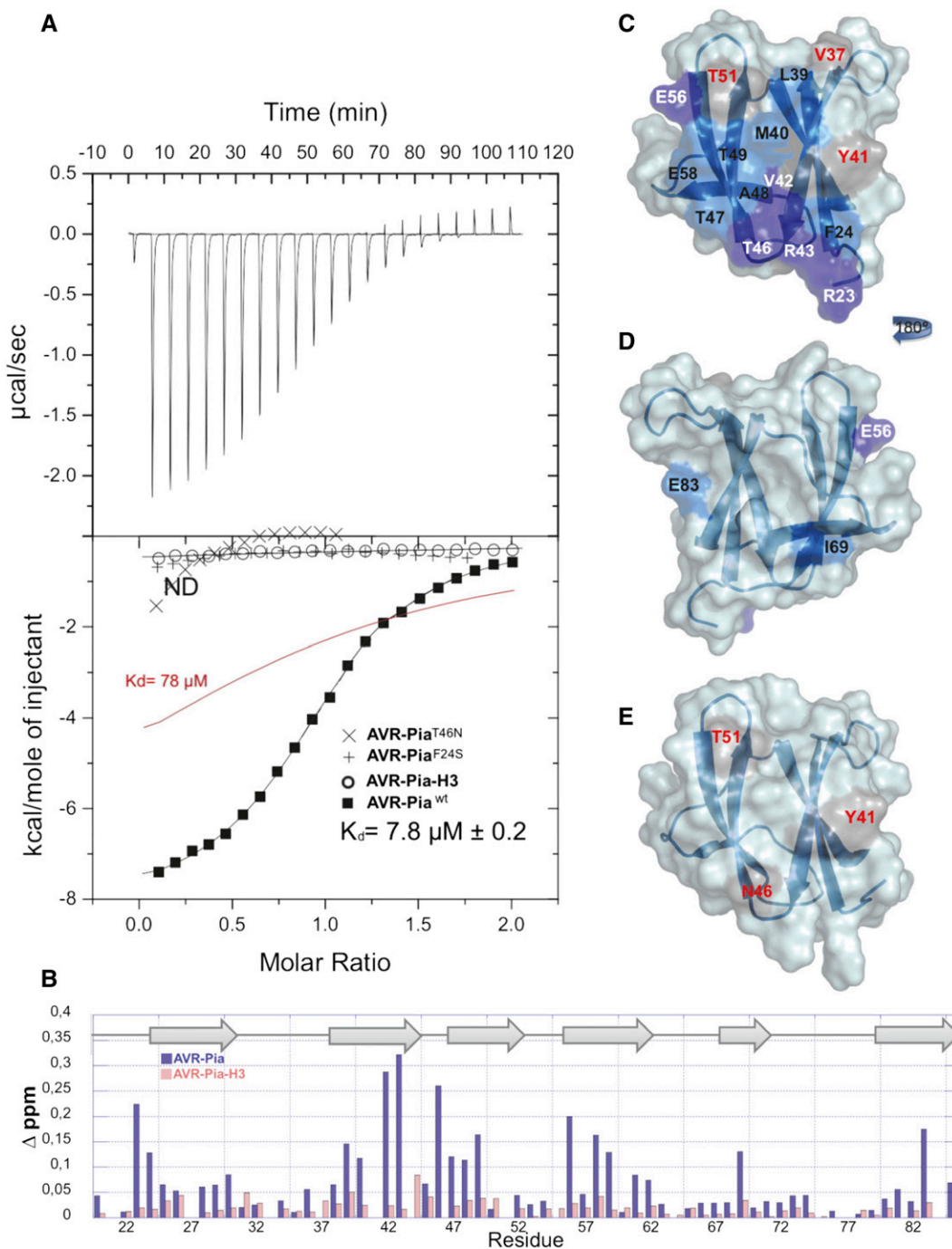


Figure 2. AVR-Pia Binds RGA5_{RATX1} with Intermediate Affinity and a Well-Defined Interaction Surface.

(A) ITC curves for the titration of the RGA5_{RATX1} domain by AVR-Pia^{wt} (squares), AVR-Pia-H3 (circles), AVR-Pia^{F24S} (+), and AVR-Pia^{T46N} (×) at 25°C. For AVR-Pia^{wt} the fit parameters were $n = 0.994 \pm 0.004$, $K_a = 1.28 \pm 0.04 \cdot 10^{-5} \text{ mol}^{-1}$, $\Delta H = -8179 \pm 47.95 \text{ cal} \cdot \text{mol}^{-1}$, $\Delta S = -4.06 \text{ cal} \cdot \text{K}^{-1} \cdot \text{mol}^{-1}$. The red line shows a simulated curve for a 10× lower affinity ($K_a = 1.28 \cdot 10^{-4} \text{ mol}^{-1}$).

(B) NMR titration and surface mapping. Plot of the chemical shift differences (Δppm) between unbound and bound AVR-Pia (blue) or AVR-Pia-H3 (red). Chemical shift differences were calculated as the Hamming distance (Schumann et al., 2007), $\Delta \delta (\text{ppm}) = |\Delta \delta(^1\text{H})_i| + 0.102 \cdot |\Delta \delta(^{15}\text{N})_i|$, where $\Delta \delta(^1\text{H})_i$ and $\Delta \delta(^{15}\text{N})_i$ are the chemical shift differences observed at $R = 0$ and $R = 2$, respectively.

(C) to (E) Structures of AVR-Pia **(C)** and **(D)** and AVR-Pia-H3 **(E)** with color-coded surfaces showing the differences in chemical shifts in the NMR titration (difference between free [$R = 0$] and RGA5_{RATX1}-bound AVR-Pia or AVR-PiaH3 [$R = 2$]). Surfaces of residues with chemical shift differences $\Delta \delta (\text{ppm}) \geq 0.2$ are shown in dark blue (residues in white letters) and in light blue for $0.2 > \Delta \delta (\text{ppm}) \geq 0.1 \text{ ppm}$ (residues in black letters). Surfaces of residues not observed in the AVR-Pia-RGA5_{RATX1} complex ($R = 2$). HSQC are reported in gray (residues in red letters), and unperturbed residues are not highlighted (residues are not indicated). The view in **(D)** is the opposite face of **(C)**, which has been rotated 180° from the vertical axis.

amino acids located on the binding surface. This results in a change of the chemical shift in NMR experiments. Depending on the rate of complex formation and dissociation, expressed by the exchange rate constant k_{ex} , and the chemical shift difference $\Delta\omega$ between the unbound and bound states ($\Delta\omega$ = difference between the resonance frequencies of the exchanging sites), different exchange regimes occur. NMR titration showed that the AVR-Pia-RGA5_{RATX1} complex was in slow exchange with $k_{ex} \ll \Delta\omega$ since separate resonances appeared for individual species (bound and unbound states) (Supplemental Figure 3A). Residues with important chemical shift changes between free AVR-Pia ($R = 0$) and AVR-Pia bound to RGA5_{RATX1} (molar ratio $R = 2$) were almost exclusively surface exposed and located in a region formed essentially by β -strands 2 and 3 and including residues R23 and F24 from β -strand 1 as well as E56 and E58 from β -strand 4 (Figures 2B and 2C). No peaks were observed for residues Y27, V37, Y41, I44, and T51 in the complex. This candidate interaction surface largely overlaps with an extended, solvent-exposed patch of hydrophobic/aromatic residues formed by F24, V26, and Y28 in β 1, V37, L38, and Y41 in β 2, and Y85 in β 6. The residues on the other side of the AVR-Pia structure were not shifted in the NMR titration and therefore seem not to be involved in the interaction with RGA5_{RATX1} (Figure 2D). Two exceptions were E83, which probably senses a perturbation of the residue Y41 that is close in space, and the I69 residue, which may be involved in local conformational rearrangement of the short β 5 strand.

RGA5_{RATX1} titration experiments were also performed with ¹⁵N-labeled AVR-Pia-H3, which shows no binding in Y2H (Césari et al., 2013) and ITC (Figure 2A) analysis. Spectral perturbations were strongly reduced and only few and limited changes of chemical shifts occurred when titrating AVR-Pia-H3 with RGA5_{RATX1} (Figures 2B and 2E; Supplemental Figure 3B). Signals for the R23, S24, V42, R43, and E83 residues were still observed at the end of the titration, while they were mostly lost at a molar ratio of 0.5 in the case of AVR-Pia (Supplemental Figure 3). Similarly, signals for E58, V59, and T47 were much less perturbed. Nevertheless, the peaks for Y41, N46, and T51 were also perturbed, indicating a weak residual interaction between RGA5_{RATX1} and AVR-Pia-H3 (Figures 2B and 2E; Supplemental Figure 3).

In summary, NMR titration identified a candidate interaction surface formed by β -strands 2 and 3 and including, in addition, residues R23, F24, E56, and E58 (Figure 2B). This surface overlaps extensively with an extended hydrophobic patch on the AVR-Pia surface that contains F24 and has T46 on its border and that may be crucial for RGA5_{RATX1} binding.

Y2H Experiments with Structure-Informed AVR-Pia Mutants Confirm an Important Role of the Candidate Interaction Surface in RGA5_{C-ter} Binding

To test whether the AVR-Pia candidate interaction surface identified *in vitro* mediates binding to RGA5_{C-ter} *in vivo*, we performed Y2H assays using AVR-Pia variants bearing point mutations in critical residues identified by NMR titration. Individual surface-exposed hydrophobic (M40, Y41, and Y85) or charged (R23, D29, R36, E56, and E58) amino acids, located in or at the border of the candidate interaction surface, were replaced by alanine. In addition, naturally occurring AVR-Pia polymorphisms located within the candidate interaction surface were tested: F24S

and T46N from AVR-Pia-H3 and R43G from AVR-Pia-H2 identified in *M. oryzae* isolates pathogenic to rice and *Setaria* species, respectively (Supplemental Figure 4A) (Césari et al., 2013). As controls, we generated mutants where surface-exposed charged residues located outside the candidate interaction surface were replaced by alanine (D63A, K67A, K74A, and D78A; Figure 3A).

As previously reported, yeasts coexpressing BD-AVR-Pia and AD-RGA5_{C-ter} or AD-RGA5_{C-ter} and BD-RGA5_{C-ter} grew on selective medium, indicating physical binding between AVR-Pia and RGA5_{C-ter}, and homo-interaction of the RGA5_{C-ter} domain (Figure 3A) (Césari et al., 2013, 2014b). Yeasts coexpressing AD-RGA5_{C-ter} and AVR-Pia^{F24S}, AVR-Pia^{R43G}, or AVR-Pia^{R36A} fused to the BD domain did not grow on selective medium, indicating that these mutations abolish binding to RGA5_{C-ter}. Isolates expressing BD fusions of the AVR-Pia variant carrying the mutation R23A, D29A, T46N, E58A, or D63A showed reduced growth compared with wild-type BD-AVR-Pia, indicating that these mutations also affect AVR-Pia-RGA5_{C-ter} interaction. By contrast, yeast clones expressing BD fusions of AVR-Pia^{Y41A}, AVR-Pia^{E56A}, AVR-Pia^{K67A}, AVR-Pia^{K74A}, or AVR-Pia^{D78A} showed similar growth as wild-type BD-AVR-Pia, while AVR-Pia^{M40A} and AVR-Pia^{Y85A} isolates showed stronger growth. All BD-AVR-Pia variants were expressed at similar levels as the wild-type BD-AVR-Pia (Figure 3B). Taken together, these Y2H data show that the replacement of all charged amino acids in the interaction surface, with the exception of E56, either abolish or reduce binding of AVR-Pia to RGA5_{C-ter} while exchanging hydrophobic residues within the interaction surface seems to abolish the interaction (in the case of F24S) or increase the binding (in the cases of M40A and Y85A).

To rule out that reduced binding of AVR-Pia mutants to RGA5_{C-ter} is due to major changes in protein structure, the AVR-Pia mutants R23A, D29A, R36A, R43G, and E58A were expressed in *Escherichia coli*, purified to homogeneity, and analyzed by ¹H-1D-NMR experiments (Supplemental Figure 4B). All mutant proteins showed similar spectra as AVR-Pia wild type, indicating that they were well structured and only locally disturbed. Recombinant AVR-Pia-D63A could not be expressed.

Taken together, these results suggest that most residues of the AVR-Pia interaction surface identified by NMR titration play an important role in RGA5_{C-ter} binding.

Co-IP Experiments Identify Key Residues in the AVR-Pia Interaction Surface That Are Crucial for RGA5_{RATX1} Binding in Planta

To investigate the role of the AVR-Pia interaction surface in *in planta* binding to RGA5_{C-ter}, coimmunoprecipitation (co-IP) experiments were performed. HA-tagged RGA5_{C-ter} and YFP-tagged AVR-Pia mutants with reduced binding in Y2H were coexpressed in *Nicotiana benthamiana* by *Agrobacterium tumefaciens*-mediated transient transformation. We also analyzed AVR-Pia^{M40A} as it has, according to Y2H experiments, increased affinity for RGA5_{C-ter}. As a negative control, a YFP fusion of the cytoplasmic *M. oryzae* effector PWL2 was used (Khang et al., 2010). Immunoblotting using anti-GFP and anti-HA antibodies showed proper expression of all proteins (Figure 4). However, AVR-Pia mutants with reduced binding to RGA5_{C-ter} in Y2H reproducibly accumulated at lower levels than AVR-Pia^{wt}, while AVR-Pia^{M40A} was expressed at similar levels (Figure 4). All YFP fusion proteins were efficiently and

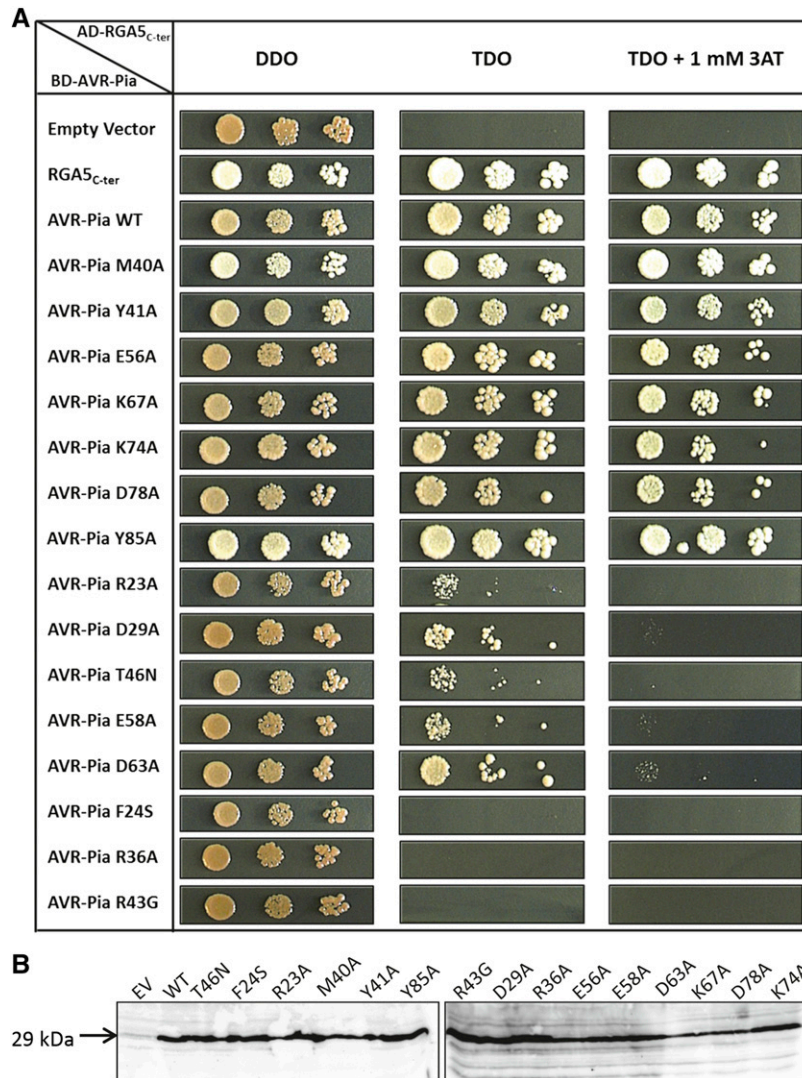


Figure 3. Mutations in the Binding Surface of AVR-Pia Affect Binding to RGA5_{C-ter} in Y2H Assays.

(A) The interaction between AVR-Pia mutants (BD fusion) and RGA5_{C-ter} (AD fusion) was assayed by a Y2H experiment. Three dilutions (1/10, 1/100, and 1/1000) of yeast cultures adjusted to an OD of 0.2 were spotted on synthetic double dropout (DDO) medium (-Trp/-Leu) to control for proper growth and on synthetic TDO (-Trp/-Leu/-His) either without or supplemented with 3-amino-1,2,4-triazole (3AT) to test for interaction. Yeast transformations and interaction analyses were performed twice with identical results. Photos were taken after 4 d of growth.

(B) Equal production of AVR-Pia mutant proteins was determined by immunoblotting with anti-AVR-Pia antibodies.

comparably precipitated with anti-GFP antibodies, but only AVR-Pia^{M40A} coprecipitated RGA5_{C-ter} as strongly as AVR-Pia^{wt}. The other mutants showed various degrees of impairment ranging from slightly (AVR-Pia^{R23A}, AVR-Pia^{E58A}, and AVR-Pia^{D63A}) to strongly (AVR-Pia^{D29A}, AVR-Pia^{R36A}, and AVR-Pia^{R43G}) reduced or even completely abolished RGA5_{C-ter} coprecipitation (AVR-Pia^{F24S}) (Figure 4A). Since the quantities of the different AVR-Pia variants after immunoprecipitation were similar to the quantity of immunoprecipitated AVR-Pia wild type, the differences in the coprecipitation of RGA5_{C-ter} reflect interaction strength and not differences in the expression levels of YFP-AVR-Pia variants. The specificity of the interactions was confirmed with PWL2 that does not interact with RGA5_{C-ter}.

It has previously been shown that the interaction of AVR-Pia with RGA5_{C-ter} relies on interaction with the RATX1 domain (RGA5_{RATX1}) (Césari et al., 2013). To verify that interaction specificities of the AVR-Pia mutants with RGA5_{C-ter} correlates with their strength of interaction with RGA5_{RATX1}, co-IP experiments were performed using HA-tagged RGA5_{RATX1}. AVR-Pia^{wt} and AVR-Pia^{M40A} strongly coprecipitated HA-RGA5_{RATX1}, while the other mutants showed reduced (R23A and D63A), strongly reduced (D29A, R36A, and E58A), or no coprecipitation of RGA5_{RATX1} (F24S and R43G) (Figure 4B).

Taken together, these data indicate that AVR-Pia^{wt} and AVR-Pia^{M40A} strongly interact with RGA5_{C-ter} and RGA5_{RATX1}, while mutants affected in direct binding to RGA5_{C-ter} in Y2H showed

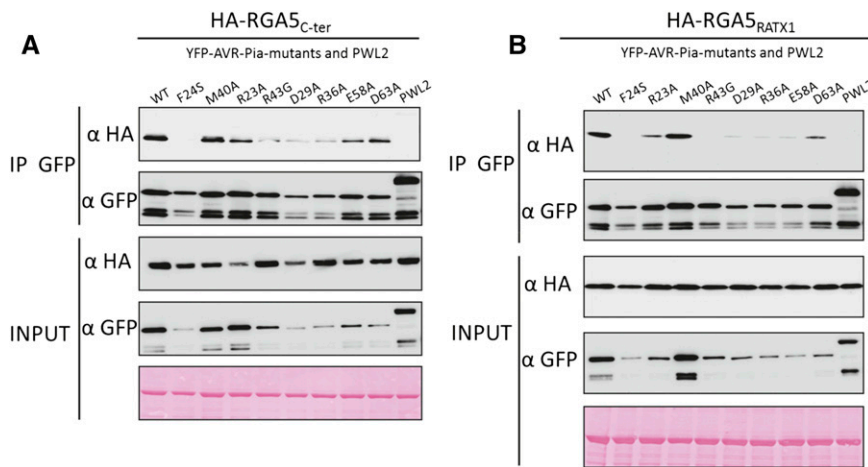


Figure 4. AVR-Pia Mutants with Reduced RGA5_{C-ter} Binding in Yeast Are Also Impaired in Binding to RGA5_{C-ter} and RGA5_{RATX1} in Planta.

HA:RGA5_{C-ter} (**A**) or HA:RGA5_{RATX1} (**B**) were transiently expressed with YFP:AVR-Pia^{WT} or YFP:AVR-Pia mutants and YFP:PWL2 in *N. benthamiana*. Protein extracts were analyzed by immunoblotting with anti-HA (α -HA) and anti-GFP antibodies (α -GFP) (Input). Immunoprecipitation (IP) was conducted with anti-GFP beads (IP GFP) and analyzed by immunoblotting with α -GFP for the detection of immunoprecipitated AVR-Pia variants. Coprecipitated HA:RGA5_{C-ter} (**A**) or HA:RGA5_{RATX1} (**B**) proteins were detected using α -HA antibody.

reduced association with RGA5_{C-ter} and RGA5_{RATX1} in planta. Complete absence of association with RGA5_{RATX1} for AVR-Pia^{F24S} and AVR-Pia^{R43G}, both in planta and in Y2H, indicates a crucial role of these residues in the binding interface and suggests that they are pivotal for AVR-Pia recognition.

Direct Binding to the RATX1 Domain Is Required for AVR-Pia Recognition

To determine the role of the RATX1 binding surface of AVR-Pia in specific recognition by the RGA4/RGA5 pair, AVR-Pia mutants were coexpressed in *N. benthamiana* with RGA4/RGA5 and cell death activation was monitored. Since tagged versions of AVR-Pia proved inactive in this assay, untagged AVR-Pia mutants were used. AVR-Pia mutants with wild-type binding to RGA5_{RATX1} induced cell death, indicating that they are recognized by RGA5/RGA4 (Supplemental Figures 5A and 5B). Weakly or nonbinding mutants lost cell death inducing activity but were also less abundant than AVR-Pia^{wt} or recognized AVR-Pia mutants (Supplemental Figures 5A to 5C). They could be detected only after enrichment by immunoprecipitation and showed in most cases only very low abundance (Supplemental Figure 5D). Therefore, no clear conclusions can be drawn for these mutants since lack of recognition may not only be due to reduced binding strength but also to low protein abundance or a combination of both effects. Differences in the protein level of AVR-Pia mutants were previously observed with YFP-tagged variants expressed in *N. benthamiana* (Figure 4) but not upon expression in *E. coli* or yeast (Figure 3B). Therefore, differences in the accumulation of AVR-Pia variants seem not related to an intrinsic destabilization of these proteins but rather to result from reduced stability in *N. benthamiana*.

Since transient heterologous experiments failed to determine the importance of the binding of AVR-Pia to RGA5_{RATX1} for recognition and disease resistance, the biological activity of AVR-Pia mutants was assayed in the homologous rice/*M. oryzae* system.

Transgenic *M. oryzae* isolates were generated that carried the different mutant alleles under the control of the constitutive RP27 promoter (RP27_{Pro}) (Bourett et al., 2002). As a control, transgenic Guy11 isolates carrying a RP27_{Pro}:mRFP construct were generated and proved to be fully virulent (Figure 5; Supplemental Figure 6B). For three different PCR-validated transgenic isolates per construct, the accumulation of AVR-Pia variants was verified in culture filtrates by immunoblotting with anti AVR-Pia antibodies (Supplemental Figure 6A). All AVR-Pia mutants were detected in at least one transgenic isolate except AVR-Pia^{D63A}, which may be unstable in *M. oryzae*. For AVR-Pia^{D29A} and AVR-Pia^{E58A}, only two and one isolate expressed the mutant protein (Supplemental Figure 6A).

The transgenic isolates were analyzed on the rice cultivars Kitaake carrying the *Pia* locus and Maratelli lacking *Pia*. All isolates were highly virulent on Maratelli, indicating that they were not affected in virulence (Supplemental Figure 6B). On Kitaake plants, the isolates expressing AVR-Pia^{wt}, AVR-Pia^{R23A}, AVR-Pia^{D29A}, AVR-Pia^{R36A}, or AVR-Pia^{E58A} were completely avirulent and produced either no symptoms or small HR lesions characteristic of resistance (Figure 5; Supplemental Figure 6B). This finding indicates that these AVR-Pia variants are fully active and recognized by RGA4/RGA5. Consistent with the absence of protein expression, AVR-Pia^{D63A} isolates did not induce resistance and were fully virulent on Kitaake plants. Isolates producing AVR-Pia^{R43G} were partially virulent and formed disease lesions characterized by a gray center that were, however, smaller and less frequent than those provoked by the control mRFP isolates. Isolates expressing AVR-Pia^{F24S} were highly virulent on Kitaake and produced large numbers of disease lesions (Figure 5; Supplemental Figure 6B).

Taken together, these results indicate that interaction of AVR-Pia with the RGA5_{RATX1} domain is required for recognition but that a reduction of this interaction as in AVR-Pia^{R23A}, AVR-Pia^{D29A}, or AVR-Pia^{E58A} does not impair recognition. Only the R43G and F24S

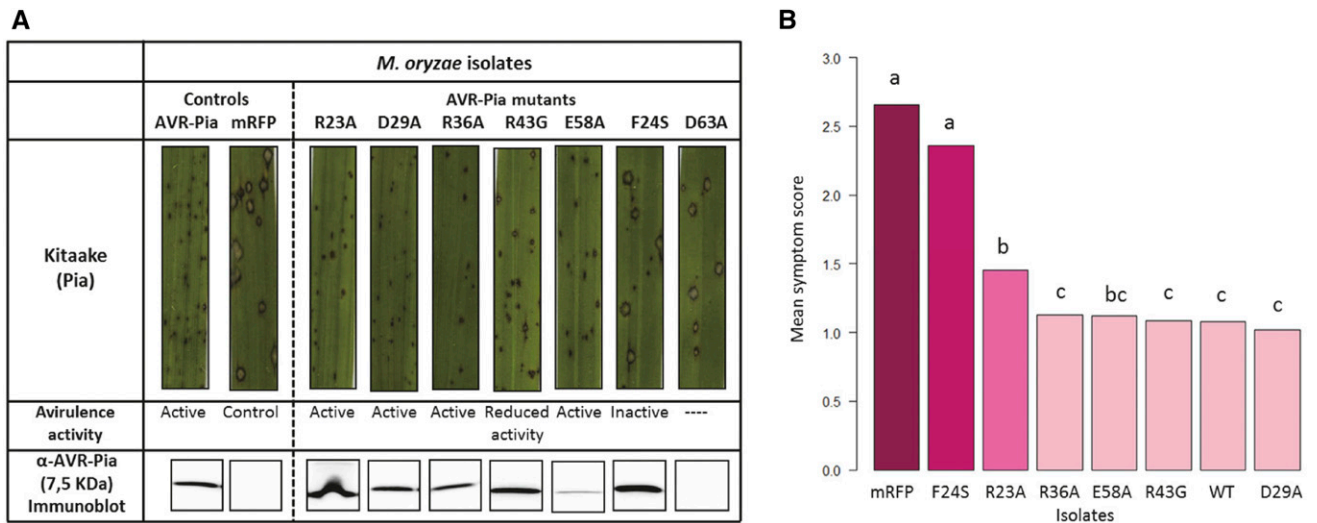


Figure 5. Effector Recognition by RGA5 Requires Binding to the RATX1 Domain.

Transgenic *M. oryzae* isolates were analyzed for the production of the AVR-Pia protein by immunoblotting using culture filtrate and α -AVR-Pia antibodies (**A**, lower panel) and were sprayed on 3-week-old plants of the rice cultivar Kitaake possessing *Pia* resistance. Seven days after inoculation, leaves were scanned (**A**, lower panel) and three different types of lesions (1 = fully resistant, 2 = partially resistant/weakly susceptible, 3 = fully susceptible) were counted on leaves from 10 different plants per isolate to determine mean symptom scores and significantly different classes of isolates using Kruskal-Wallis analysis of variance combined with a multicomparison Dunn test for nonparametric data (**B**). The AVR-Pia variants grouped with respect to their avirulence activity in three significantly different classes: a = inactive; b = partially active; c = active. Similar results were obtained in two independent experiments and with additional transgenic isolates.

polymorphisms that abolished RGA5_{RATX1} interaction both in planta and in yeast affected AVR-Pia recognition, with AVR-Pia^{F24S} being completely inactive.

AVR-Pia Associates with RGA5 Outside of the RATX1 Domain

The high resilience of RGA4/RGA5-mediated AVR-Pia recognition to reduction of AVR-Pia-RGA5_{RATX1} interaction strength suggested that AVR-Pia might interact with additional sites in RGA5. To test this hypothesis, in planta association of the AVR-Pia mutants with the RGA5 full-length protein was assayed by co-IP. All AVR-Pia mutants, including AVR-Pia^{F24S} and AVR-Pia^{R43G}, coprecipitated RGA5 as efficiently as AVR-Pia^{wt} (Figure 6A). This indicates that lack of binding to RGA5_{RATX1} does not abolish association with RGA5. It also further confirms that the lower expression level of some AVR-Pia variants is not limiting for interaction in co-IP experiments and that the reduced coprecipitation of RGA5_{RATX1} and RGA5_{C-ter} (Figure 4) truly reflects reduced interaction strength and is not related to sometimes low expression levels of AVR-Pia variants. To test whether association of AVR-Pia with RGA5 is truly independent of the RATX1 domain, interaction of AVR-Pia with an RGA5 construct lacking the RATX1 domain (RGA5 Δ RATX1) was tested by co-IP. All AVR-Pia variants coprecipitated RGA5 Δ RATX1 (Figure 6B) and AVR-Pia mutants with reduced or no binding to RGA5_{RATX1} interacted as strongly with RGA5 Δ RATX1 as AVR-Pia^{wt}, demonstrating that the RATX1 domain is not necessary for formation of RGA5/AVR-Pia complexes. These results suggest that AVR-Pia interacts with additional sites in RGA5 outside of the RATX1 domain and that the region of AVR-Pia that mediates association with RGA5 Δ RATX1 lies outside of the RATX1 binding surface.

It was previously shown that RGA5 Δ RATX1 inhibits RGA4-triggered cell death and, therefore, that the RATX1 domain is not required for RGA5-mediated repression of RGA4 (Césari et al., 2014b). Since AVR-Pia still associates with RGA5 Δ RATX1 in planta, we tested whether AVR-Pia would be recognized by RGA5 Δ RATX1/RGA4 and trigger cell death independently of the RATX1 domain. Neither coexpression of RGA4, RGA5 Δ RATX1, and AVR-Pia nor expression of these three proteins together with the isolated RATX1 domain triggered cell death (Supplemental Figure 7). This finding indicates that association of AVR-Pia with regions outside of the RATX1 domain is not sufficient to release RGA5-mediated RGA4 repression and further confirms that binding of AVR-Pia to RGA5_{RATX1} is required for derepression of RGA4. In addition, these results suggest that AVR-Pia has to interact with the RATX1 domain in the context of the full-length RGA5 protein since an isolated RATX1 domain does not complement RGA5 Δ RATX1 for AVR-Pia recognition.

DISCUSSION

Identification of a RGA5_{RATX1} Binding Surface in AVR-Pia

In this study, we provide evidence that AVR-Pia interacts with the RATX1 domain of RGA5 through a precise binding surface consisting of β -strands 2 and 3, residues R23 and F24 from β -strand 1, and residues E56 and E58 from β -strand 4 (Figure 2C). This interaction surface, identified by NMR titration experiments with recombinant AVR-Pia and the RATX1 domain, was confirmed by mutant analysis. Indeed, replacement of residues R23, F24, D29, R43, T46, or E58 strongly reduced or abolished binding to

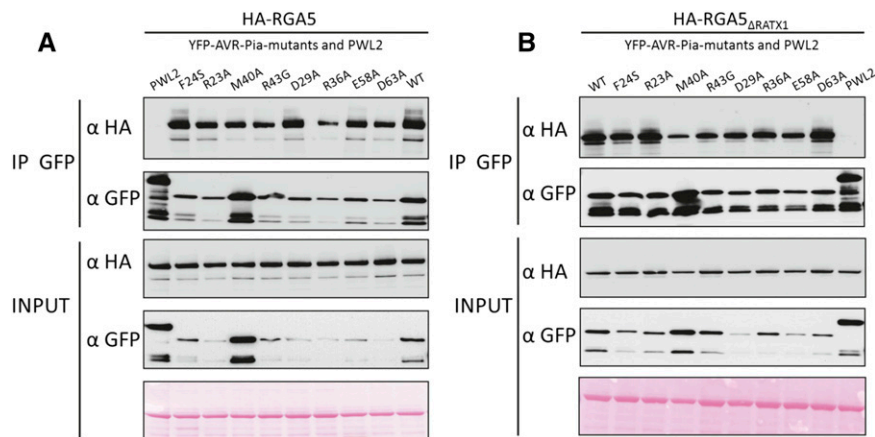


Figure 6. AVR-Pia Associates with RGA5 outside the RATX1 Domain.

HA:RGA5 (**A**) and HA:RGA5 $_{\Delta$ RATX1 (**B**) were expressed with YFP:AVR-Pia^{WT} or YFP:AVR-Pia mutants and YFP:PwL2 in *N. benthamiana*. Protein extracts were analyzed by immunoblotting with anti-HA (α -HA) and anti-GFP antibodies (α -GFP) (Input). Immunoprecipitation (IP) was conducted with anti-GFP beads (IP GFP) and analyzed by immunoblotting with α -GFP for the detection of immunoprecipitated AVR-Pia variants. Coprecipitated RGA5 (**A**) or HA:RGA5 $_{\Delta$ RATX1 (**B**) were detected using α -HA antibody.

RGA5 $_{\text{RATX1}}$ in Y2H and co-IP experiments, while replacement of residues M40 and Y85 increased interaction in Y2H (Figures 3 and 4). Substitutions outside of the candidate interaction surface had no effect on binding, with the exception of residues R36 and D63. Residue R36 is located in the loop joining β 1 and β 2 and might also be involved in RATX1 binding since its mutation causes reduced association with the RGA5 $_{\text{RATX1}}$ domain. Alternatively, it may play an important role in defining the positions of β -strands 1, 2, and 6 through the salt bridge it forms with residue E83 in β 6. The D63A polymorphism seems to destabilize the overall structure since AVR-Pia^{D63A} could not be expressed in *E. coli* or *M. oryzae*. In fact, D63 seems important to the structure of the β 4- β 5 loop as its side-chain carboxyl group forms a hydrogen bond with the side-chain amid group of N65. This may be required for the proper positioning of C66, which forms a disulfide bridge with C25 linking the two β sheets β 1, β 2, β 6 and β 3, β 4, β 5 and thereby influences global folding.

AVR-Pia and AVR-PikD Have Distinct RATX1/HMA Binding Surfaces That Are Situated at Similar Positions

The three-dimensional structure of a AVR-PikD-Pikp-1_{HMA} complex was determined by crystallography and showed that, like the formation of the AVR-Pia-RGA5 $_{\text{RATX1}}$ complex, binding of AVR-PikD to Pikp-1_{HMA} involves β -strands 2 and 3 (Supplemental Figure 8A) (Maqbool et al., 2015). However, in AVR-PikD, the residues of β -strand 2 that are crucial for Pikp-1_{HMA} binding, R64 and D66, are charged and establish hydrogen bonds and salt bridge interactions, respectively. By contrast, in AVR-Pia, surface-exposed residues of β -strand 2 are hydrophobic and probably establish hydrophobic interactions (Figure 2C). In addition, unlike AVR-Pia, AVR-PikD possesses an N-terminal extension of 32 amino acids that is crucial for physical binding to Pikp-1_{HMA} and recognition by Pikp-1/Pikp-2 (Supplemental Figure 8B). In particular, residue H46 from this extension establishes important interactions with matching residues in Pikp-1_{HMA}. These interactions are

necessary for binding and, together with the neighboring residues P47 and G48, for matching specificities with alleles of Pikp-1 (Kanzaki et al., 2012; Maqbool et al., 2015). These residues are missing in AVR-Pia but similarly important interactions are established with the amino acid F24 from the very hydrophobic β -strand 1. Therefore, recognition of the sequence-unrelated, but structurally similar, effectors AVR-Pia and AVR-PikD seems to involve similar structural elements but relies on distinct and highly specific mechanisms.

Whether the effector interaction surfaces of the RATX1/HMA domains of RGA5 and Pikp-1 are similar or completely different remains an open question. Crystal structures show that Pikp-1_{HMA} has a typical HMA α / β -sandwich fold, composed of two α -helices and a four-stranded antiparallel β -sheet, that mediates interaction with AVR-PikD (Supplemental Figure 8C) (Maqbool et al., 2015). We used molecular modeling to evaluate whether AVR-Pia binding may involve similar regions in RGA5 $_{\text{RATX1}}$ but no consensus docking model could be generated for the AVR-Pia-RGA5 $_{\text{RATX1}}$ complex (Supplemental Figure 8C). Interestingly, none of the docking models predicted an interaction surface in RGA5 $_{\text{RATX1}}$ similar to the effector binding surface of Pikp-1_{HMA}. This suggests that the RGA5 $_{\text{RATX1}}$ -AVR-Pia complex differs significantly from the Pikp-1_{HMA}-AVR-Pik-D complex.

Taken together, recognition of the structurally similar MAX effectors AVR-Pia and AVR-Pik by independently acquired NLR-integrated HMA domains seems to rely on distinct molecular mechanisms. Future work is required to test this hypothesis through functional studies of the Pikp-1_{HMA} interaction surface identified by structural analysis and the identification of the surface that mediates effector binding in RGA5 $_{\text{RATX1}}$.

Binding of AVR-Pia to the Integrated RATX1 Domain Is Required for Recognition but Is of Moderate Affinity

The mutants AVR-Pia^{F24S} and AVR-Pia^{R43A} showed drastically reduced RGA5 $_{\text{RATX1}}$ binding and triggered no or reduced resistance,

respectively, indicating that the AVR-Pia-RGA5_{RATX1} interaction is required for RGA4/RGA5-mediated recognition. The presence of these polymorphisms in naturally occurring AVR-Pia alleles (Ribot et al., 2013) suggests that in rice isolates of *M. oryzae*, AVR-Pia is undergoing selection for mutations in the RATX1-interaction surface and escape from RGA4/RGA5-mediated recognition. These results therefore provide further support for a crucial role of nonconventional, integrated decoy domains in effector recognition and NLR specificity.

However, we also found high resilience of AVR-Pia recognition to a reduction in RGA5_{RATX1} binding strength since the weakly binding AVR-Pia mutants AVR-Pia^{R23A}, AVR-Pia^{E58A}, AVR-Pia^{D29A}, and AVR-Pia^{R36A} were still able to trigger resistance. Similar observations were made regarding AVR-PikD, the only other example where the affinity of an effector to the integrated decoy domain of its NLR receptor has been determined (Maqbool et al., 2015). Indeed, AVR-PikD^{A67D} and AVR-PikD^{P47A G48D} mutants showed drastically reduced binding to Pikp-1_{HMA} but were nevertheless perfectly well recognized by Pik-1/Pik-2.

A possible explanation for this tolerance to a reduction in the affinity between effectors and integrated decoys could be that effectors interact with multiple independent sites in NLR receptors. Indeed, our study suggests that, besides the RATX1 domain, AVR-Pia interacts with other, not yet defined, regions in RGA5. In the simplest case, this interaction relies on direct physical binding, but since it was solely detected by co-IP experiments, the possibility that the binding is indirect and involves additional cofactors cannot be excluded. This interaction seems mediated by other AVR-Pia surfaces than those involved in RGA5_{RATX1} binding since mutants with reduced binding to RGA5_{RATX1} are not affected in interaction with RGA5_{ΔRATX1}. As the RATX1 domain is covalently linked to the rest of the RGA5 receptor, AVR-Pia binding to these other sites has the potential to increase the overall effector binding affinity to RGA5 despite the low affinity binding to RGA5_{RATX1} ($K_d = 7 \mu\text{M}$). In this context, further mutation-induced reduction of AVR-Pia affinity toward the RATX1 domain may not have a dramatic effect unless it completely abolishes AVR-Pia/RGA5_{RATX1} interaction. This situation highlights an advantage of the

integration of the decoy domain into the NLR receptor over a situation where the decoy is a separate molecule and has to bind to the effector before subsequent binding to the NLR receptor. In the latter case, low affinity of the effector-decoy interaction would lead to drastically reduced receptor occupancy and render the corresponding resistance more vulnerable to effector mutations affecting decoy binding.

Interaction of Effectors with Multiple Independent Sites Is a Hallmark of NLR Receptor Activation

Effector recognition by RGA4/RGA5 differs from other well-studied NLR models. Indeed, RGA5 has no inherent signaling activity and functions, on the one hand, by repressing RGA4 signaling activity and, on the other, by releasing repression upon AVR-Pia binding (Césari et al., 2014a). Interestingly, the RATX1 domain is required only for derepression and not for repression (Supplemental Figure 7) (Césari et al., 2014b). Providing the RATX1 domain separately in the presence of RGA5_{ΔRATX1} and AVR-Pia does not relieve repression despite the fact that AVR-Pia interacts with the separate partners, RGA5_{ΔRATX1} and RGA5_{RATX1} (Supplemental Figure 7). To explain this result, we propose the hypothesis that simultaneous binding of AVR-Pia to different sites in RGA5, including the RATX1 domain, is required to trap RGA5 in a conformation unable to repress RGA4 (Figure 7).

That effectors have to establish simultaneously several independent interactions with NLRs or NLRs and cofactors to be recognized and trigger resistance has been frequently observed with effectors from various origins (Collier and Moffett, 2009). In the *Pseudomonas syringae* effector AvrRPS4, two different surface areas on opposite and distant sites of the molecule are required for recognition by the RRS1/RPS4 pair (Sohn et al., 2012). One of these sites is crucial for binding to the integrated WRKY decoy domain of RRS1, while the other seems to interact with other not yet identified regions in RRS1 (Sarris et al., 2015). Similarly, recognition of the *Hyaloperonospora arabidopsidis* effector ATR1-EMOY2 by the NLRs RPP1-NdA or RPP1-WsB from Arabidopsis relies on two different surface areas from two

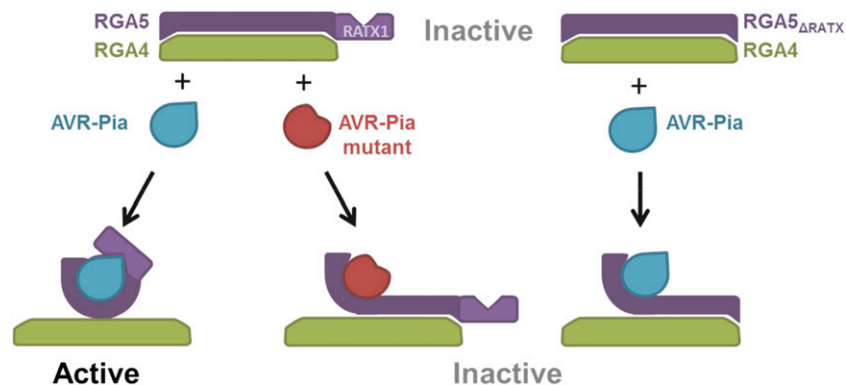


Figure 7. Model of AVR-Pia Recognition by the RGA4/RGA5 Receptor Complex.

AVR-Pia binds to the RATX1 domain of RGA5 with a defined interaction surface and interacts, in addition, through independent surfaces with other sites in RGA5. These additional interactions are not sufficient to relieve the repression RGA5 exerts on RGA4. Indeed, AVR-Pia mutants that associate with RGA5, but do not bind RGA5_{RATX1} as well as RGA5 mutants that lack the RATX1 domain, do not permit activation of resistance. We propose that simultaneous interactions of AVR-Pia with different parts of RGA5, including the RATX1 domain, stabilize conformational changes that activate the RGA4/RGA5 complex.

different domains and on opposite sides of the molecule, suggesting simultaneous interaction with independent binding sides in RPP1-NdA and RPP1WsB (Chou et al., 2011; Steinbrenner et al., 2015). Also in NLRs that recognize effector-cofactor complexes, simultaneous binding of these complexes to different parts of the NLR, generally involving the N terminus and the leucine-rich repeat have been frequently described (Collier and Moffett, 2009). Therefore, we propose the hypothesis that effectors or effector-cofactor complexes forcing or trapping NLRs in an activated state by simultaneously binding to multiple binding sites and inducing or stabilizing by this major conformational changes is a widespread mechanism in NLR activation and particularly in NLRs with integrated domains. Future structural and functional analysis will be necessary to test this model and elucidate in more detail how activation occurs at the molecular level.

METHODS

Growth Conditions of Plants and Fungi and Infection Assays

Nicotiana benthamiana plants were grown in a growth chamber at 22°C under fluorescent light (Radium; fluorescent lamp Spectralux Plus NL-T8 58W/865/G13) with a 16-h light period. Rice plants (*Oryza sativa*) were grown as described (Faivre-Rampant et al., 2008). Transgenic *Magnaporthe oryzae* GUY 11 strains were grown at 25°C during 5 d on rice flour agar for spore production (Berruyer et al., 2003) and in Tanaka complete culture medium (Villalba et al., 2008) agitated at 60 rpm and 25°C during 5 d for liquid culture.

For the analysis of interaction phenotypes, a suspension of *M. oryzae* conidiospores in water with 0.1% of gelatin and adjusted to 5×10^4 spores mL^{-1} was sprayed on the leaves of 3-week-old rice plants (Berruyer et al., 2003). Symptoms were analyzed 7 d after inoculation on the youngest leaf that was fully expanded at the time of inoculation. For quantitative analysis, lesions were classified and counted: resistant lesions, visible as small brown spots (type 1); weakly susceptible/partially resistant lesions characterized by a pronounced brown border and a small gray center (type 2); fully susceptible lesions characterized by a large gray center (type 3).

Constructs

Plasmids were generated by Gateway cloning (Thermo Fisher), restriction/ligation, site-directed mutagenesis using the QuickChange Lightning kit (Agilent), or gap-repair cloning in yeast (Bruno et al., 2004). Gateway entry clones were generated using the pDONR207 plasmid (Thermo Fisher). Gateway destination vectors were modified pBIN19 plasmids for expression of tagged proteins in *N. benthamiana* (Césari et al. 2013) or modified pGAD-T7 or pGBK-T7 plasmids (Clontech) for yeast two-hybrid experiments (Bernoux et al., 2011). For protein expression, the pET-15b vector (Merck-Millipore) was used. For *M. oryzae* transformation, constructs were based on the pDL02 plasmid (Bruno et al., 2004). For details on PCR and mutagenesis primers and generation of plasmids, refer to Supplemental Tables 2 and 3.

NMR Spectroscopy and Structure Determination

Spectra were acquired on a 700 MHz Avance Bruker spectrometer equipped with triple-resonance (^1H , ^{15}N , ^{13}C) z-gradient cryoprobe at 305K. All spectra are referenced to the internal reference DSS for the ^1H dimension and indirectly referenced for the ^{15}N and ^{13}C dimensions (Wishart et al., 1995).

Spectra were processed using Topspin (version 3.2) and analyzed using strip-plots with Cindy in house software and CCPN (Vranken et al., 2005) (analysis v 2.3). The ^1H , ^{15}N , and ^{13}C assignments were derived by analogy from the assignments of AVR-Pia wild type without the need to prepare

a ^{13}C -labeled sample and the details are given in Supplemental Methods. Briefly, one protein preparation of ^{15}N -labeled AVR-Pia-H3 in water was used to record 3D ^{15}N - ^1H experiments for backbone assignments and 2D NOESY and 2D TOCSY for side-chain assignments. To solve ambiguous assignments and to obtain ^{13}C chemical shift data, the sample was lyophilized and dissolved in D_2O , and ^{13}C - ^1H HSQC/TOCSY experiments were recorded. Distance restraints obtained from the 3D ^{15}N -NOESY-HSQC and 2D-NOESY spectra, Φ/Ψ dihedral angle constraints from TALOS+ (Shen et al., 2009), and H-bonds were used to generate structures by CYANA (Güntert, 2004), CNS (Brunger, 2007), and the refinement in water of RECOORD (Nederveen et al., 2005) (Supplemental Table 1 and Supplemental Methods).

NMR Titration

For the assignments, protein samples (1 mM) in 20 mM potassium-sodium phosphate, pH 5.4, and 150 mM NaCl were used. For the titrations of ^{15}N -labeled AVR-Pia proteins, different samples with constant concentrations of AVR-Pia wild type or H3 (50 μM) and various concentrations of unlabeled RATX1 (ratios 2:1, 1:1, 0.5:1, 0.25:1, and 0:1 for the reference) were prepared. HSQC spectra were recorded at 305K on a Bruker Avance 700 MHz spectrometer. Chemical shift differences were measured from the HSQC spectra of AVR-Pia or AVR-H3 alone and the AVR-RATX1 complex at $R = 2$. They are reported as Hamming distance weighted by the magnetogyric ratios (Schumann et al., 2007).

Co-IP and Y2H Interaction Assays

Protein-protein interaction analyses by coimmunoprecipitation were performed with protein extracts from *N. benthamiana* leaf discs harvested 2 d after Agrobacterium infiltration (Césari et al., 2013). For the interaction of AVR-Pia variants with RGA5_{C-ter} and RGA5_{RATX1}, five leaf disks per sample were homogenized in extraction buffer (25 mM Tris-HCl, pH 7.5, 150 mM NaCl, 1 mM EDTA, 10 mM DTT, 1 mM PMSF, and 0.1% IGEPAL CA-630 [Nonidet P-40]), supplemented with complete protease inhibitor cocktail (Roche) and polyvinylpyrrolidone (PVPP; 0.5%). After two centrifugations (30 min, 15,000g), 5 μL magnetic GFP-trap_M beads (Chromotek) per sample washed two times with protein extraction buffer (without PVPP) were added to 500 μL protein extract and incubated with gentle rotation for 2 h at 4°C. Beads were separated and washed three times with 600 μL protein extraction buffer (without PVPP).

For the interaction of AVR-Pia variants and RGA5 or RGA5_{RATX1}, a modified protein extraction buffer was used (50 mM Tris-HCl, pH 7.5, 150 mM NaCl, 1 mM EDTA, 10 mM DTT, 1 mM PMSF, 1.0% IGEPAL CA-630 [Nonidet P-40], 0.5% sodium deoxycholate, and 0.1% SDS, supplemented with a complete protease inhibitor cocktail [Roche] and 0.5% PVPP). Co-IP was performed with 8 μL agarose GFP_trap_A suspension (Chromotek) and four washes with the modified protein extraction buffer.

Bound proteins were eluted by boiling for 10 min at 70°C in 50 μL NuPAGE sample buffer, separated by polyacrylamide gel electrophoresis using NuPAGE 4 to 12% gels (Invitrogen), transferred to nitrocellulose membrane (Millipore), and analyzed by immunoblotting. For immunodetection of proteins, rat anti-HA-horseradish peroxidase (clone 3F10; Sigma-Aldrich) or mouse anti-GFP (clones 7.1 and 13.1, Sigma-Aldrich) and goat anti-mouse-horseradish peroxidase (Sigma-Aldrich) were used in combination with the Immobilon western kit (Millipore).

Binding domain (BD) fusions of AVR-Pia variants in pGBK7-53 and activation domain (AD) fusions of RGA5_{C-ter} in pGAD7 were transformed in gold and Y187 yeast strain, respectively. Interactions assays were performed according to the Matchmaker Gold yeast two-hybrid system protocol (Clontech).

Transient Protein Expression and HR Assays in *N. benthamiana*

For agroinfiltration in *N. benthamiana*, pBIN19 binary vectors containing either AVR-Pia, PWL2, or RGA5 variants were transformed into Agrobacterium strain

GV3101 by electroporation. Individual clones were selected and grown in Luria-Bertani liquid medium containing 50 mg mL⁻¹ rifampicin, 15 mg mL⁻¹ gentamycin, and 50 mg mL⁻¹ kanamycin at 28°C for 24 h before agroinfiltration. Coinoculation mixtures adjusted to an OD₆₀₀ of 1.0 were infiltrated in 4-week-old *N. benthamiana* plants. The infiltrated plants were incubated for 48 or 96 h in growth chambers under controlled conditions for coimmunoprecipitations or cell death assays, respectively. Three days after infiltration, *N. benthamiana* leaves were scanned using a Typhoon FLA9000 fluorescence scanner (GE Healthcare) with excitation at 635 nm and a long-pass red filter (LPR-665 nm) to evaluate the HR response as a lack of red chlorophyll fluorescence.

Accession Numbers

Sequence data from this article correspond to those previously published (Césari, et al., 2013) and can be found in the GenBank/EMBL databases under the following accession numbers: AVR-Pia (AB498873), AVR-Pia-H3 (KC777366), PWL2 (U26313), RGA4 (AB604622), Sasanishiki RGA5-A (AB604627), and Sasanishiki RGA5-B (KC777365). The Protein Data Bank accession number for the AVR-Pia_H3 structure is 5JHJ.

Supplemental Data

- Supplemental Figure 1.** Solution structure of AVR-Pia-H3.
- Supplemental Figure 2.** Comparison of NMR relaxation of AVR-Pia and AVR-Pia-H3.
- Supplemental Figure 3.** HSQC spectra of AVR-Pia and AVR-Pia-H3 recorded upon titration with RGA5_{RATX1}.
- Supplemental Figure 4.** AVR-Pia mutants affected in RGA5_{RATX1} binding are well structured.
- Supplemental Figure 5.** AVR-Pia mutants not affected in RGA5_{RATX1} binding trigger HR in *N. benthamiana*.
- Supplemental Figure 6.** Characterization of transgenic *M. oryzae* isolates carrying AVR-Pia mutant constructs.
- Supplemental Figure 7.** RGA5_{ΔRATX1} represses RGA4-mediated cell death but does not recognize AVR-Pia.
- Supplemental Figure 8.** Comparison of the AVR-Pia and AVR-PikD structures and their complexes with RATX1/HMA domains.
- Supplemental Table 1.** Statistics for 20 NMR structures of AVR-Pia-H3.
- Supplemental Table 2.** Primers.
- Supplemental Table 3.** Plasmids.
- Supplemental Methods.** Supplemental experimental procedures and methods.

ACKNOWLEDGMENTS

This work was supported by the French Infrastructure for Integrated Structural Biology (ANR-10-INSB-05-0) and the ANR project Immunereceptor (ANR-15-CE20-0007). D.O. was supported by a PhD grant from the Ministry of Research of Colombia (Colciencias). This work benefited from interactions promoted by COST Action FA 1208 (<https://www.cost-sustain.org>). We thank Christian Roumestand for fruitful discussions.

AUTHOR CONTRIBUTIONS

T.K. and A.P. acquired funding and conceived, supervised, and designed the research. D.O., J.G., K.G., V.C., and A.P. conducted the investigation. D.O., A.P., and T.K. wrote the original draft. D.O., A.P., S.C., and T.K. wrote,

reviewed, and edited the article. D.O. and S.C. provided resources and generated vectors. D.O., S.C., K.G., V.C., and A.P. performed the research. A.P. and K.G. performed NMR analyses. D.O. and V.C. produced transgenic *M. oryzae* strains. D.O. performed protein-protein interaction analyses. D.O., J.G., K.G., A.P., and T.K. analyzed data. D.O., T.K., and A.P. wrote the article

Received June 9, 2016; revised November 9, 2016; accepted January 12, 2017; published January 13, 2017.

REFERENCES

- Bernoux, M., Ve, T., Williams, S., Warren, C., Hatters, D., Valkov, E., Zhang, X., Ellis, J.G., Kobe, B., and Dodds, P.N.** (2011). Structural and functional analysis of a plant resistance protein TIR domain reveals interfaces for self-association, signaling, and auto-regulation. *Cell Host Microbe* **9**: 200–211.
- Berruyer, R., Adreit, H., Milazzo, J., Gaillard, S., Berger, A., Dioh, W., Lebrun, M.-H.H., and Tharreau, D.** (2003). Identification and fine mapping of Pi33, the rice resistance gene corresponding to the *Magnaporthe grisea* avirulence gene ACE1. *Theor. Appl. Genet.* **107**: 1139–1147.
- Bonardi, V., Tang, S., Stallmann, A., Roberts, M., Cherkis, K., and Dangl, J.L.** (2011). Expanded functions for a family of plant intracellular immune receptors beyond specific recognition of pathogen effectors. *Proc. Natl. Acad. Sci. USA* **108**: 16463–16468.
- Bourett, T.M., Sweigard, J.A., Czymmek, K.J., Carroll, A., and Howard, R.J.** (2002). Reef coral fluorescent proteins for visualizing fungal pathogens. *Fungal Genet. Biol.* **37**: 211–220.
- Brunger, A.T.** (2007). Version 1.2 of the crystallography and NMR system. *Nat. Protoc.* **2**: 2728–2733.
- Bruno, K.S., Tenjo, F., Li, L., Hamer, J.E., Xu, J., and Ai, B.E.T.** (2004). Cellular localization and role of kinase activity of PMK1 in *Magnaporthe grisea*. **3**: 1525–1532.
- Césari, S., et al.** (2013). The rice resistance protein pair RGA4/RGA5 recognizes the *Magnaporthe oryzae* effectors AVR-Pia and AVR1-CO39 by direct binding. *Plant Cell* **25**: 1463–1481.
- Césari, S., Bernoux, M., Moncuquet, P., Kroj, T., and Dodds, P.N.** (2014a). A novel conserved mechanism for plant NLR protein pairs: the “integrated decoy” hypothesis. *Front. Plant Sci.* **5**: 606.
- Césari, S., Kanzaki, H., Fujiwara, T., Bernoux, M., Chalvon, V., Kawano, Y., Shimamoto, K., Dodds, P., Terauchi, R., and Kroj, T.** (2014b). The NB-LRR proteins RGA4 and RGA5 interact functionally and physically to confer disease resistance. *EMBO J.* **33**: 1941–1959.
- Chou, S., Krasileva, K.V., Holton, J.M., Steinbrener, A.D., Alber, T., and Staskawicz, B.J.** (2011). *Hyaloperonospora arabidopsidis* ATR1 effector is a repeat protein with distributed recognition surfaces. *Proc. Natl. Acad. Sci. USA* **108**: 13323–13328.
- Collier, S.M., and Moffett, P.** (2009). NB-LRRs work a “bait and switch” on pathogens. *Trends Plant Sci.* **14**: 521–529.
- Cui, H., Tsuda, K., and Parker, J.E.** (2015). Effector-triggered immunity: from pathogen perception to robust defense. *Annu. Rev. Plant Biol.* **66**: 487–511.
- Dean, R., Van Kan, J.A., Pretorius, Z.A., Hammond-Kosack, K.E., Di Pietro, A., Spanu, P.D., Rudd, J.J., Dickman, M., Kahmann, R., Ellis, J., and Foster, G.D.** (2012). The top 10 fungal pathogens in molecular plant pathology. *Mol. Plant Pathol.* **13**: 414–430.
- de Guillen, K., Ortiz-Vallejo, D., Gracy, J., Fournier, E., Kroj, T., and Padilla, A.** (2015). Structure analysis uncovers a highly diverse but structurally conserved effector family in phytopathogenic fungi. *PLoS Pathog.* **11**: e1005228.
- Eitas, T.K., and Dangl, J.L.** (2010). NB-LRR proteins: pairs, pieces, perception, partners, and pathways. *Curr. Opin. Plant Biol.* **13**: 472–477.

- Ellis, J.G., Dodds, P.N., and Lawrence, G.J. (2007). Flax rust resistance gene specificity is based on direct resistance-avirulence protein interactions. *Annu. Rev. Phytopathol.* **45**: 289–306.
- Favre-Rampant, O., Thomas, J., Allègre, M., Morel, J.-B., Tharreau, D., Nottèghem, J.-L., Lebrun, M.-H., Schaffrath, U., and Piffanelli, P. (2008). Characterization of the model system rice-Magnaporthe for the study of nonhost resistance in cereals. *New Phytol.* **180**: 899–910.
- Fukuoka, S., Saka, N., Koga, H., Ono, K., Shimizu, T., Ebana, K., Hayashi, N., Takahashi, A., Hirochika, H., Okuno, K., and Yano, M. (2009). Loss of function of a proline-containing protein confers durable disease resistance in rice. *Science* **325**: 998–1001.
- Gabriëls, S.H.E.J., Vossen, J.H., Ekengren, S.K., van Ooijen, G., Abd-El-Halim, A.M., van den Berg, G.C.M., Rainey, D.Y., Martin, G.B., Takken, F.L.W., de Wit, P.J.G.M., and Joosten, M.H. (2007). An NB-LRR protein required for HR signalling mediated by both extra- and intracellular resistance proteins. *Plant J.* **50**: 14–28.
- Güntert, P. (2004). Automated NMR structure calculation with CYANA. *Methods Mol. Biol.* **278**: 353–378.
- Jacob, F., Vernaldi, S., and Maekawa, T. (2013). Evolution and conservation of plant NLR functions. *Front. Immunol.* **4**: 297.
- Jia, Y., McAdams, S.A., Bryan, G.T., Hershey, H.P., and Valent, B. (2000). Direct interaction of resistance gene and avirulence gene products confers rice blast resistance. *EMBO J.* **19**: 4004–4014.
- Kanzaki, H., Yoshida, K., Saitoh, H., Fujisaki, K., Hirabuchi, A., Alaux, L., Fournier, E., Tharreau, D., and Terauchi, R. (2012). Arms race co-evolution of *Magnaporthe oryzae* AVR-Pik and rice Pik genes driven by their physical interactions. *Plant J.* **72**: 894–907.
- Khang, C.H., Berruyer, R., Giraldo, M.C., Kankanala, P., Park, S.-Y., Czymbek, K., Kang, S., and Valent, B. (2010). Translocation of *Magnaporthe oryzae* effectors into rice cells and their subsequent cell-to-cell movement. *Plant Cell* **22**: 1388–1403.
- Krasileva, K.V., Dahlbeck, D., and Staskawicz, B.J. (2010). Activation of an Arabidopsis resistance protein is specified by the in planta association of its leucine-rich repeat domain with the cognate oomycete effector. *Plant Cell* **22**: 2444–2458.
- Liu, W., Liu, J., Triplett, L., Leach, J.E., and Wang, G.-L. (2014). Novel insights into rice innate immunity against bacterial and fungal pathogens. *Annu. Rev. Phytopathol.* **52**: 213–241.
- Maekawa, T., et al. (2011). Coiled-coil domain-dependent homodimerization of intracellular barley immune receptors defines a minimal functional module for triggering cell death. *Cell Host Microbe* **9**: 187–199.
- Maqbool, A., Saitoh, H., Franceschetti, M., Stevenson, C., Uemura, A., Kanzaki, H., Kamoun, S., Terauchi, R., and Banfield, M. (2015). Structural basis of pathogen recognition by an integrated HMA domain in a plant NLR immune receptor. *Elife* **4**: 1–24.
- Nyarko, A., Singarapu, K.K., Figueroa, M., Manning, V.A., Pandelova, I., Wolpert, T.J., Ciuffetti, L.M., and Barbar, E. (2014). Solution NMR structures of Pyrenophora tritici-repentis ToxB and its inactive homolog reveal potential determinants of toxin activity. *J. Biol. Chem.* **289**: 25946–25956.
- Okuyama, Y., et al. (2011). A multifaceted genomics approach allows the isolation of the rice Pia-blast resistance gene consisting of two adjacent NBS-LRR protein genes. *Plant J.* **66**: 467–479.
- Pennisi, E. (2010). Armed and dangerous. *Science* **327**: 804–805.
- Qi, D., and Innes, R.W. (2013). Recent advances in plant NLR structure, function, localization, and signaling. *Front. Immunol.* **4**: 348.
- Ribot, C., Césari, S., Abidi, I., Chalvon, V., Bournaud, C., Vallet, J., Lebrun, M.-H., Morel, J.-B., and Kroj, T. (2013). The Magnaporthe oryzae effector AVR1-CO39 is translocated into rice cells independently of a fungal-derived machinery. *Plant J.* **74**: 1–12.
- Le Roux, C., et al. (2015). A receptor pair with an integrated decoy converts pathogen disabling of transcription factors to immunity. *Cell* **161**: 1074–1088.
- Nederveen, A.J., et al. (2005). RECOORD: A recalculated coordinate database of 500+ proteins from the PDB using restraints from the BioMagResBank. *Proteins* **59**: 662–672.
- Sarris, P.F.F., et al. (2015). A plant immune receptor detects pathogen effectors that target WRKY transcription factors. *Cell* **161**: 1089–1100.
- Schumann, F.H., Riepl, H., Maurer, T., Gronwald, W., Neidig, K.P., and Kalbitzer, H.R. (2007). Combined chemical shift changes and amino acid specific chemical shift mapping of protein-protein interactions. *J. Biomol. NMR* **39**: 275–289.
- Shen, Y., Delaglio, F., Cornilescu, G., and Bax, A. (2009). TALOS+: a hybrid method for predicting protein backbone torsion angles from NMR chemical shifts. *J. Biomol. NMR* **44**: 213–223.
- Skamnioti, P., and Gurr, S.J. (2009). Against the grain: safeguarding rice from rice blast disease. *Trends Biotechnol.* **27**: 141–150.
- Sohn, K.H., Hughes, R.K., Piquerez, S.J., Jones, J.D.G., and Banfield, M.J. (2012). Distinct regions of the *Pseudomonas syringae* coiled-coil effector AvrRps4 are required for activation of immunity. *Proc. Natl. Acad. Sci. USA* **109**: 16371–16376.
- Steinbrenner, A.D., Goritschnig, S., and Staskawicz, B.J. (2015). Recognition and activation domains contribute to allele-specific responses of an Arabidopsis NLR receptor to an oomycete effector protein. *PLoS Pathog.* **11**: e1004665.
- Takken, F.L.W., and Goverse, A. (2012). How to build a pathogen detector: structural basis of NB-LRR function. *Curr. Opin. Plant Biol.* **15**: 375–384.
- van der Hoorn, R.A.L., and Kamoun, S. (2008). From Guard to Decoy: a new model for perception of plant pathogen effectors. *Plant Cell* **20**: 2009–2017.
- Villalba, F., Collemare, J., Landraud, P., Lambou, K., Brozek, V., Cirer, B., Morin, D., Bruel, C., Beffa, R., and Lebrun, M.-H. (2008). Improved gene targeting in *Magnaporthe grisea* by inactivation of MgKU80 required for non-homologous end joining. *Fungal Genet. Biol.* **45**: 68–75.
- Vranken, W.F., Boucher, W., Stevens, T.J., Fogh, R.H., Pajon, A., Llinas, M., Ulrich, E.L., Markley, J.L., Ionides, J., and Laue, E.D. (2005). The CCPN data model for NMR spectroscopy: development of a software pipeline. *Proteins* **59**: 687–696.
- Williams, S.J., et al. (2014). Structural basis for assembly and function of a heterodimeric plant immune receptor. *Science* **344**: 299–303.
- Wishart, D.S., Bigam, C.G., Yao, J., Abildgaard, F., Dyson, H.J., Oldfield, E., Markley, J.L., and Sykes, B.D. (1995). 1H, 13C and 15N chemical shift referencing in biomolecular NMR. *J. Biomol. NMR* **6**: 135–140.
- Wu, C.-H., Belhaj, K., Bozkurt, T.O., Birk, M.S., and Kamoun, S. (2016). Helper NLR proteins NRC2a/b and NRC3 but not NRC1 are required for Pto-mediated cell death and resistance in Nicotiana benthamiana. *New Phytol.* **209**: 1344–1352.
- Zhang, Z.-M., Zhang, X., Zhou, Z.-R., Hu, H.-Y., Liu, M., Zhou, B., and Zhou, J. (2013). Solution structure of the *Magnaporthe oryzae* avirulence protein AvrPiz-t. *J. Biomol. NMR* **55**: 219–223.

Recognition of the *Magnaporthe oryzae* Effector AVR-Pia by the Decoy Domain of the Rice NLR Immune Receptor RGA5

Diana Ortiz, Karine de Guillen, Stella Cesari, Véronique Chalvon, Jérôme Gracy, André Padilla and Thomas Kroj

Plant Cell 2017;29;156-168; originally published online January 13, 2017;
DOI 10.1105/tpc.16.00435

This information is current as of March 27, 2017

Supplemental Data	http://www.plantcell.org/content/suppl/2017/01/13/tpc.16.00435.DC1.html http://www.plantcell.org/content/suppl/2017/02/06/tpc.16.00435.DC2.html
References	This article cites 44 articles, 12 of which can be accessed free at: http://www.plantcell.org/content/29/1/156.full.html#ref-list-1
Permissions	https://www.copyright.com/ccc/openurl.do?sid=pd_hw1532298X&issn=1532298X&WT.mc_id=pd_hw1532298X
eTOCs	Sign up for eTOCs at: http://www.plantcell.org/cgi/alerts/ctmain
CiteTrack Alerts	Sign up for CiteTrack Alerts at: http://www.plantcell.org/cgi/alerts/ctmain
Subscription Information	Subscription Information for <i>The Plant Cell</i> and <i>Plant Physiology</i> is available at: http://www.aspb.org/publications/subscriptions.cfm